Plane Poiseuille flow of a rarefied gas in the presence of strong gravitation

Toshiyuki Doi*

Department of Applied Mathematics and Physics, Graduate School of Engineering, Tottori University, Tottori 680-8552, Japan

(Received 9 October 2010; revised manuscript received 8 December 2010; published 28 February 2011)

Plane Poiseuille flow of a rarefied gas, which flows horizontally in the presence of strong gravitation, is studied based on the Boltzmann equation. Applying the asymptotic analysis for a small variation in the flow direction [Y. Sone, *Molecular Gas Dynamics* (Birkhäuser, 2007)], the two-dimensional problem is reduced to a one-dimensional problem, as in the case of a Poiseuille flow in the absence of gravitation, and the solution is obtained in a semianalytical form. The reduced one-dimensional problem is solved numerically for a hard sphere molecular gas over a wide range of the gas-rarefaction degree and the gravitational strength. The presence of gravitation reduces the mass flow rate, and the effect of gravitation is significant for large Knudsen numbers. To verify the validity of the asymptotic solution, a two-dimensional problem of a flow through a long channel is directly solved numerically, and the validity of the asymptotic solution is confirmed.

DOI: 10.1103/PhysRevE.83.026311 PACS number(s): 47.61.−k, 47.45.Ab, 51.10.+y

I. INTRODUCTION

Poiseuille flow is a fundamental and important problem in rarefied gas dynamics and has been studied very comprehensively based on the Boltzmann equation [1–14]. Although this research extends over five decades and the accumulation of the relevant studies is considerable, studies even on the fundamental part are still under development [15]. Usually the flow is considered in the absence of gravitation because gravity of the earth is so weak that its effect on the flow may be negligible. However, in an atmospheric gas flow at a very high altitude, where the characteristic length and the mean-free path of the gas can both be large, the effect of gravity can be significant. Thus, understanding of the effect of gravitation on the flow behavior based on the kinetic study is necessary.

Studies of channel flow subject to an external force may be classified into two categories: flow that is parallel or perpendicular to the force. The first case concerns a flow through a vertical channel or pipe that is induced by gravitation [16–25]. This problem interests many scientists because the temperature field induced by the flow exhibits an interesting profile. In Ref. [24], the systematic asymptotic analysis of the Boltzmann equation for a small Knudsen number is conducted, the temperature profile is explained analytically, and the ghost effect of an infinitesimally weak gravity on the flow in the continuum limit is clarified. The second case concerns the influence of gravity on channel or pipe flows that flow horizontally. Santos and coworkers have studied the influence of gravity on the heat flow problem extensively based on the Boltzmann equation using a perturbation method [26–28]. As an extension of their analysis, they studied the influence of weak gravity on the horizontal shear flow in Ref. [28]. However, studies on this second case are not as extensive as those on the first case, and, to the author's knowledge, Refs. [28,29] are the only relevant studies on this subject based on the Boltzmann equation.

In the present study, we consider a time-independent plane Poiseuille flow of a rarefied gas that flows horizontally and is subject to strong gravitation. Here *strong* means that the height by which molecules ascend against gravity is comparable to the channel width and the mean-free path of the gas. To be specific, this problem contains four characteristic lengths: the channel width, the mean-free path of the gas molecules, the ascent height of molecules, and the length scale in which the pressure varies appreciably in the flow direction. In this study, we consider the case in which the first three of the characteristic lengths are comparable, whereas the last is much larger than the others. In this situation, the asymptotic analysis [30–33] of the Boltzmann equation for a small variation in the longitudinal direction may be applicable. Thanks to the asymptotic analysis, the structure of the solution is resolved, and the problem is reduced to a one-dimensional problem. The reduced one-dimensional problem is solved numerically for a hard sphere molecular gas over a wide range of gas rarefaction degree and gravitational strength. Based on the numerical solution, we discuss the influence of gravity on the Poiseuille flow for an arbitrary but finite gas rarefaction degree and gravitational strength.

The present paper is organized as follows. In Sec. II the problem and the basic equation are stated. In Sec. III the asymptotic analysis is conducted. In Sec. IV the results of the numerical analysis of the reduced one-dimensional problem are presented. In Sec. V, to verify the validity of the asymptotic solution, a two-dimensional flow problem through a long channel is directly solved numerically, and the validity of the asymptotic solution is discussed. This paper ends with a conclusion in Sec. VI.

II. PROBLEM AND BASIC EQUATION

A. Problem

Let us consider a rarefied gas between two plane parallel walls placed at rest at $X_2 = 0$ and $X_2 = L$, where X_i is the space rectangular coordinates. The temperature of the walls is uniform and equal to T_0. The gas is subject to uniform gravitation $(0, -g, 0)$. There is a pressure gradient in the X_1 direction, and a flow is induced owing to this pressure gradient. We study the time-independent behavior of the gas under the following assumptions: (i) the gas behavior is governed by the Boltzmann equation, (ii) the gas molecules undergo diffuse reflection on the walls, and (iii) the pressure gradient in the horizontal direction X_1 is so small that the quantities vary slowly in this direction.

*doi@damp.tottori-u.ac.jp

B. Basic equation

Take L, T_0, and ρ_0 as the reference length, the reference temperature, and the reference density of the system, where ρ_0 is an arbitrary constant having the dimension of the density. We introduce the dimensionless variables x_i, ζ_i, and $\hat{f}$ for the space coordinates X_i, the molecular velocity ξ_i, and the velocity distribution function f as

$$x_i = \frac{X_i}{L}, \quad \zeta_i = \frac{\xi_i}{(2RT_0)^{1/2}}, \quad \hat{f} = \frac{f}{\rho_0(2RT_0)^{-3/2}}, \tag{1}$$

where R is the specific gas constant, i.e., the Boltzmann constant divided by the mass m of a molecule. The time-independent Boltzmann equation for the spatially two-dimensional case is written in the dimensionless form as

$$\zeta_1 \frac{\partial \hat{f}}{\partial x_1} + \zeta_2 \frac{\partial \hat{f}}{\partial x_2} - \hat{g}\frac{\partial \hat{f}}{\partial \zeta_2} = \frac{2}{\sqrt{\pi}\mathrm{Kn}}\hat{J}(\hat{f},\hat{f}), \tag{2}$$

$$\hat{J}(\hat{f},\hat{f}) = \iint (\hat{f}'_*\hat{f}' - \hat{f}_*\hat{f})\hat{B}\, d\hat{\Omega}(\boldsymbol{\alpha})\, \boldsymbol{d\zeta}_*, \tag{3}$$

where

$$\begin{gathered} \hat{f} = f(\mathbf{x}, \boldsymbol{\zeta}), \quad \hat{f}_* = f(\mathbf{x}, \boldsymbol{\zeta}_*), \quad \hat{f}' = f(\mathbf{x}, \boldsymbol{\zeta}'), \\ \hat{f}'_* = f(\mathbf{x}, \boldsymbol{\zeta}'_*), \\ \boldsymbol{\zeta}' = \boldsymbol{\zeta} + [\boldsymbol{\alpha}\cdot(\boldsymbol{\zeta}_* - \boldsymbol{\zeta})]\boldsymbol{\alpha}, \quad \boldsymbol{\zeta}'_* = \boldsymbol{\zeta}_* - [\boldsymbol{\alpha}\cdot(\boldsymbol{\zeta}_* - \boldsymbol{\zeta})]\boldsymbol{\alpha}, \end{gathered} \tag{4}$$

$\boldsymbol{\alpha}$ is a unit vector, $d\hat{\Omega}(\boldsymbol{\alpha})$ is the solid-angle element in the direction of $\boldsymbol{\alpha}$, and $\boldsymbol{d\zeta}_* = d\zeta_{1*}\, d\zeta_{2*}\, d\zeta_{3*}$. $\hat{B}$ is a function of $|\boldsymbol{\alpha}\cdot(\boldsymbol{\zeta}_* - \boldsymbol{\zeta})|/|\boldsymbol{\zeta}_* - \boldsymbol{\zeta}|$ and $|\boldsymbol{\zeta}_* - \boldsymbol{\zeta}|$, and its functional form is determined by the molecular model. The integration in Eq. (3) is carried out over the entire direction of $\boldsymbol{\alpha}$ and the entire space of $\boldsymbol{\zeta}$. $\mathrm{Kn} = \ell_0/L$ is the Knudsen number, in which $\ell_0 = 1/(\sqrt{2}\pi d_m^2 m^{-1}\rho_0)$ is the mean-free path of the gas in the equilibrium state at rest with the density ρ_0, and d_m is the diameter of a molecule. $\hat{g} = gL/(2RT_0)$ is the dimensionless gravity.

The diffuse reflection boundary condition is written in the dimensionless form as

$$\hat{f} = \left(-2\sqrt{\pi}\int_{\zeta_{2*}<0} \zeta_{2*}\hat{f}_*\, \boldsymbol{d\zeta}_*\right) E(\boldsymbol{\zeta}) \quad (x_2 = 0, \zeta_2 > 0), \tag{5}$$

$$\hat{f} = \left(2\sqrt{\pi}\int_{\zeta_{2*}>0} \zeta_{2*}\hat{f}_*\, \boldsymbol{d\zeta}_*\right) E(\boldsymbol{\zeta}) \quad (x_2 = 1, \zeta_2 < 0), \tag{6}$$

where

$$E(\boldsymbol{\zeta}) = \pi^{-3/2}\exp(-\boldsymbol{\zeta}^2). \tag{7}$$

The macroscopic variables of the gas, the density ρ, the flow velocity v_i, the temperature T, the pressure p, the stress tensor p_{ij}, and the heat flow vector q_i are defined by the moments of the velocity distribution function. The corresponding dimensionless variables $\hat{\rho} = \rho/\rho_0$, $\hat{v}_i = v_i/(2RT_0)^{1/2}$, $\hat{T} = T/T_0$, $\hat{p} = p/p_0$, $\hat{p}_{ij} = p_{ij}/p_0$, $\hat{q}_i = q_i/[p_0(2RT_0)^{1/2}]$, where $p_0 = R\rho_0 T_0$, are given as

$$\hat{\rho} = \int \hat{f}\, \boldsymbol{d\zeta}, \tag{8}$$

$$\hat{v}_i = \frac{1}{\hat{\rho}}\int \zeta_i \hat{f}\, \boldsymbol{d\zeta}, \tag{9}$$

$$\hat{T} = \frac{2}{3\hat{\rho}}\int (\zeta_i - \hat{v}_i)^2 \hat{f}\, \boldsymbol{d\zeta}, \tag{10}$$

$$\hat{p} = \hat{\rho}\hat{T}, \tag{11}$$

$$\hat{p}_{ij} = 2\int (\zeta_i - \hat{v}_i)(\zeta_j - \hat{v}_j)\hat{f}\, \boldsymbol{d\zeta}, \tag{12}$$

$$\hat{q}_i = \int (\zeta_i - \hat{v}_i)(\zeta_j - \hat{v}_j)^2 \hat{f}\, \boldsymbol{d\zeta}. \tag{13}$$

The mass flow rate M and the heat flow rate H of the gas through a cross section per unit time and per unit width in the X_3 direction are given as

$$M = \int_0^L \rho v_1\, dX_2, \quad H = \int_0^L q_1\, dX_2, \tag{14}$$

and are expressed in terms of the dimensionless variables as

$$\frac{M}{2p_0(2RT_0)^{-1/2}L} = \int_0^1 \hat{\rho}\hat{v}_1\, dx_2, \tag{15}$$

$$\frac{H}{p_0(2RT_0)^{1/2}L} = \int_0^1 \hat{q}_1\, dx_2. \tag{16}$$

The boundary value problem (2), (5), and (6) contains two dimensionless parameters:

$$\mathrm{Kn} = \frac{\ell_0}{L} \quad \text{and} \quad \hat{g} = \frac{gL}{2RT_0}. \tag{17}$$

In addition, the pressure gradient in the longitudinal direction is small:

$$\frac{1}{\hat{p}}\left|\frac{\partial \hat{p}}{\partial x_1}\right| \ll 1. \tag{18}$$

We study the boundary value problem (2), (5), and (6) for arbitrary but finite values of Kn and $\hat{g}$ under the condition (18).

Here we comment on the dimensionless gravity parameter $\hat{g}$. In an ordinary room condition on the earth, this parameter is usually very small, e.g., $\hat{g} \sim 10^{-4}$ when $L =$ 1 m. Thus the condition of finite $\hat{g}$, for example, $\hat{g} = 0.1$, is an extreme condition of very strong gravitation that would be experienced on a planet whose gravity is a thousand times stronger than that of the earth.

III. ASYMPTOTIC ANALYSIS

In this section, we conduct an asymptotic analysis [30] of the boundary value problem (2), (5), and (6) for a small variation in the flow direction x_1. We assume that the variation of the variables in the flow direction x_1 is small and of the order of ε, i.e., $\partial\hat{f}/\partial x_1 \sim \varepsilon\hat{f}$ whereas $\partial\hat{f}/\partial x_2 \sim \hat{f}$. To deal with this behavior, we use the shrunk coordinate χ instead of x_1:

$$\chi = \varepsilon x_1. \tag{19}$$

With this new variable, the Boltzmann equation (2) becomes

$$\varepsilon\zeta_1\frac{\partial \hat{f}}{\partial \chi} + \zeta_2\frac{\partial \hat{f}}{\partial x_2} - \hat{g}\frac{\partial \hat{f}}{\partial \zeta_2} = \frac{2}{\sqrt{\pi}\mathrm{Kn}}\hat{J}(\hat{f},\hat{f}). \tag{20}$$

We seek the solution $\hat{f}$ in a power series in ε:

$$\hat{f} = \hat{f}_{(0)} + \hat{f}_{(1)}\varepsilon + \cdots. \tag{21}$$

Substituting the expansion (21) into the Boltzmann equation (20), we have

$$\zeta_2 \frac{\partial \hat{f}_{(0)}}{\partial x_2} - \hat{g}\frac{\partial \hat{f}_{(0)}}{\partial \zeta_2} - \frac{2}{\sqrt{\pi}\mathrm{Kn}}\hat{J}(\hat{f}_{(0)},\hat{f}_{(0)}) = 0, \tag{22}$$

$$\zeta_2 \frac{\partial \hat{f}_{(1)}}{\partial x_2} - \hat{g}\frac{\partial \hat{f}_{(1)}}{\partial \zeta_2} - \frac{4}{\sqrt{\pi}\mathrm{Kn}}\hat{J}(\hat{f}_{(0)},\hat{f}_{(1)}) = -\zeta_1 \frac{\partial \hat{f}_{(0)}}{\partial \chi}, \tag{23}$$

$$\cdots\cdots,$$

and the boundary conditions are

$$\hat{f}_{(0)} = \left(-2\sqrt{\pi}\int_{\zeta_{2*}<0} \zeta_{2*}\hat{f}_{(0)*}\, \boldsymbol{d\zeta}_*\right) E(\boldsymbol{\zeta}) \quad (x_2 = 0, \zeta_2 > 0), \tag{24}$$

$$\hat{f}_{(0)} = \left(2\sqrt{\pi}\int_{\zeta_{2*}>0} \zeta_{2*}\hat{f}_{(0)*}\, \boldsymbol{d\zeta}_*\right) E(\boldsymbol{\zeta}) \quad (x_2 = 1, \zeta_2 < 0), \tag{25}$$

$$\hat{f}_{(1)} = \left(-2\sqrt{\pi}\int_{\zeta_{2*}<0} \zeta_{2*}\hat{f}_{(1)*}\, \boldsymbol{d\zeta}_*\right) E(\boldsymbol{\zeta}) \quad (x_2 = 0, \zeta_2 > 0), \tag{26}$$

$$\hat{f}_{(1)} = \left(2\sqrt{\pi}\int_{\zeta_{2*}>0} \zeta_{2*}\hat{f}_{(1)*}\, \boldsymbol{d\zeta}_*\right) E(\boldsymbol{\zeta}) \quad (x_2 = 1, \zeta_2 < 0), \tag{27}$$

$$\cdots\cdots.$$

Equations (22), (24), and (25) constitute the system for the leading-order solution $\hat{f}_{(0)}$. In contrast to the analysis in the absence of an external force, Eq. (22) is a full Boltzmann equation with derivative terms with respect to not only x_2 but also ζ_2, and this problem must be solved first. Fortunately, a solution of the system (22), (24), and (25) is well known, and we immediately have

$$\hat{f}_{(0)} = C(\chi)\omega(x_2)E(\boldsymbol{\zeta}), \tag{28}$$

where

$$\omega(x_2) = \exp(-2\hat{g}x_2), \tag{29}$$

and $C(\chi)$ is an arbitrary function of χ. Solution (28) expresses the density stratification of the gas. The $C(\chi)$ appearing in (28) is undetermined at this stage and will be determined in the next-order analysis. Because the leading-order solution $\hat{f}_{(0)}$ is a Maxwellian, we can proceed with the analysis consistently. Moreover, this is a Maxwellian at rest with a *uniform* temperature, so that, as we will see, the following analysis becomes considerably simple.

Equations (23), (26), and (27) form the boundary value problem for $\hat{f}_{(1)}$. We seek the solution $\hat{f}_{(1)}$ in the form $\hat{f}_{(1)} = \hat{f}_{(0)}\phi$. Because the collision integral $\hat{J}$ has the following property [see Eq. (A.110a) in Ref. [30]]:

$$2\hat{J}(E, E\phi) = E\mathcal{L}(\phi), \tag{30}$$

where $\mathcal{L}(*)$ is the linearized collision integral defined by

$$\mathcal{L}(\phi) = \iint E_*(\phi'_* + \phi' - \phi_* - \phi)\hat{B}\, d\hat{\Omega}(\boldsymbol{\alpha})\, \boldsymbol{d\zeta}_*, \tag{31}$$

we have

$$2\hat{J}(\hat{f}_{(0)}, \hat{f}_{(0)}\phi) = 2\hat{J}[C(\chi)\omega(x_2)E(\boldsymbol{\zeta}), C(\chi)\omega(x_2)E(\boldsymbol{\zeta})\phi] = [C(\chi)\omega(x_2)]^2 E\mathcal{L}(\phi), \tag{32}$$

and thus Eq. (23) reduces to

$$\zeta_2 \frac{\partial \phi}{\partial x_2} - \hat{g}\frac{\partial \phi}{\partial \zeta_2} - \frac{2}{\sqrt{\pi}}\frac{\Omega C(\chi)}{\mathrm{Kn}}\frac{\omega(x_2)}{\Omega}\mathcal{L}(\phi) = -\frac{\zeta_1}{C(\chi)}\frac{dC(\chi)}{d\chi}. \tag{33}$$

In Eq. (33), we introduced the constant Ω:

$$\Omega = \int_0^1 \omega(x_2)\, dx_2 = [1 - \exp(-2\hat{g})]/(2\hat{g}), \tag{34}$$

which is not necessary at this stage but will be convenient in the following arrangement. The boundary conditions are

$$\phi = -2\sqrt{\pi}\int_{\zeta_{2*}<0} \zeta_{2*}\phi_* E_*\, \boldsymbol{d\zeta}_* \quad (x_2 = 0, \zeta_2 > 0), \tag{35}$$

$$\phi = 2\sqrt{\pi}\int_{\zeta_{2*}>0} \zeta_{2*}\phi_* E_*\, \boldsymbol{d\zeta}_* \quad (x_2 = 1, \zeta_2 < 0). \tag{36}$$

The variable χ enters the problem (33), (35), and (36) only through $C(\chi)$. From the linearity, the solution is given as

$$\phi(\chi, x_2, \boldsymbol{\zeta}; \mathrm{Kn}, \hat{g}) = \frac{1}{C(\chi)}\frac{dC(\chi)}{d\chi}\varphi(x_2, \boldsymbol{\zeta}; \mathrm{Kn}/[\Omega C(\chi)], \hat{g}), \tag{37}$$

where $\varphi(x_2, \boldsymbol{\zeta}; K, \hat{g})$ is the solution of the following boundary value problem

$$\zeta_2 \frac{\partial \varphi}{\partial x_2} - \hat{g}\frac{\partial \varphi}{\partial \zeta_2} - \frac{2}{\sqrt{\pi}}\frac{\omega(x_2)/\Omega}{K}\mathcal{L}(\varphi) = -\zeta_1, \tag{38}$$

$$\varphi = -2\sqrt{\pi}\int_{\zeta_{2*}<0} \zeta_{2*}\varphi_* E_*\, \boldsymbol{d\zeta}_* \quad (x_2 = 0, \zeta_2 > 0), \tag{39}$$

$$\varphi = 2\sqrt{\pi}\int_{\zeta_{2*}>0} \zeta_{2*}\varphi_* E_*\, \boldsymbol{d\zeta}_* \quad (x_2 = 1, \zeta_2 < 0). \tag{40}$$

Furthermore, we see that the following similarity solution is applicable [30,34]:

$$\varphi(x_2, \boldsymbol{\zeta}; K, \hat{g}) = \zeta_1 \Phi(x_2, \zeta_2, \zeta_\rho; K, \hat{g}), \tag{41}$$

where $\zeta_\rho = (\zeta_1^2 + \zeta_3^2)^{1/2}$. Owing to the similarity solution, the boundary value problem (38) –(40) reduces to

$$\zeta_2 \frac{\partial \Phi}{\partial x_2} - \hat{g}\frac{\partial \Phi}{\partial \zeta_2} - \frac{2}{\sqrt{\pi}}\frac{\omega(x_2)/\Omega}{K\zeta_1}\mathcal{L}(\zeta_1\Phi) = -1, \tag{42}$$

$$\Phi = 0 \quad (x_2 = 0, \zeta_2 > 0) \quad \text{and} \quad (x_2 = 1, \zeta_2 < 0). \tag{43}$$

With the aid of the solution Φ, the solution ϕ is given as

$$\phi(\chi, x_2, \boldsymbol{\zeta}; \mathrm{Kn}, \hat{g}) = \frac{1}{C(\chi)}\frac{dC(\chi)}{d\chi}\zeta_1 \Phi(x_2, \zeta_2, \zeta_\rho; \mathrm{Kn}/[\Omega C(\chi)], \hat{g}). \tag{44}$$

Collecting the results Eqs. (28) and (44), the solution $\hat{f}$ is given as

$$\hat{f} = C(\chi)\omega(x_2)E + \frac{dC(\chi)}{d\chi}\omega(x_2)\zeta_1 \Phi E\varepsilon + \cdots. \tag{45}$$

Substituting Eq. (45) into Eqs. (8)–(13), the macroscopic variables are given as

$$\hat{\rho} = C(\chi)\omega(x_2) + \cdots, \tag{46}$$

$$\hat{v}_1 = \frac{1}{C(\chi)}\frac{dC(\chi)}{d\chi}u_{\rm PG}(x_2)\varepsilon + \cdots, \tag{47}$$

$$\hat{T} = 1 + \cdots, \tag{48}$$

$$\hat{p} = C(\chi)\omega(x_2) + \cdots, \tag{49}$$

$$\hat{q}_1 = \Omega\frac{dC(\chi)}{d\chi}Q_{\rm PG}(x_2)\varepsilon + \cdots, \tag{50}$$

where

$$u_{\rm PG}(x_2;K,\hat{g}) = \pi^{-1/2}\int_{-\infty}^{\infty}\int_{0}^{\infty}\zeta_\rho^3\exp\left(-\zeta_2^2-\zeta_\rho^2\right) \times \Phi(x_2,\zeta_2,\zeta_\rho;K,\hat{g})\,d\zeta_\rho\,d\zeta_2, \tag{51}$$

$$Q_{\rm PG}(x_2;K,\hat{g}) = \pi^{-1/2}\Omega^{-1}\omega(x_2)\int_{-\infty}^{\infty}\int_{0}^{\infty}\zeta_\rho^3\left(\zeta_2^2+\zeta_\rho^2-\frac{5}{2}\right) \times \exp\left(-\zeta_2^2-\zeta_\rho^2\right)\Phi(x_2,\zeta_2,\zeta_\rho;K,\hat{g})\,d\zeta_\rho\,d\zeta_2, \tag{52}$$

and $\cdots$ are the terms of $O(\varepsilon^2)$ and higher. $\hat{v}_2,\hat{v}_3,\hat{q}_2$, and $\hat{q}_3$ are higher order in ε. Recalling $\chi = \varepsilon x_1$, we have $\varepsilon(dC/d\chi)/C = (dc/dx_1)/c$, where $c(x_1)$ is defined by $c(x_1) = C(\varepsilon x_1)$. In terms of $c(x_1)$, Eqs. (46)–(49) are written as

$$\hat{p} = \hat{\rho} = c(x_1)\omega(x_2), \tag{53}$$

$$\hat{T} = 1, \tag{54}$$

$$\hat{v}_1 = \frac{1}{c(x_1)}\frac{dc(x_1)}{dx_1}u_{\rm PG}\left(x_2;\frac{\rm Kn}{\Omega c(x_1)},\hat{g}\right), \tag{55}$$

$$\hat{q}_1 = \Omega\frac{dc(x_1)}{dx_1}Q_{\rm PG}\left(x_2;\frac{\rm Kn}{\Omega c(x_1)},\hat{g}\right), \tag{56}$$

and $\hat{v}_2 = \hat{v}_3 = \hat{q}_2 = \hat{q}_3 = 0$, where the terms of $O(\varepsilon^2)$ and the higher are neglected. This result does not contain ε as it should be. At this stage, we see that $c(x_1)$ is the dimensionless pressure $\hat{p}(x_1,0)$ at the bottom $x_2 = 0$ and that the ratio $(\partial\hat{p}/\partial x_1)/\hat{p}$ is independent of x_2. However, it is more convenient to introduce the average pressure p_a averaged over the cross section $X_1 = X_1$:

$$p_a(X_1) = \frac{1}{L}\int_0^L p\,dX_2 \tag{57}$$

and its dimensionless counterpart

$$\hat{p}_a(x_1) = p_a/p_0 = \Omega c(x_1), \tag{58}$$

where Eq. (53) is used. In terms of $\hat{p}_a$, Eqs. (53)–(56) reduce to a more familiar form

$$\hat{p} = \hat{\rho} = \hat{p}_a(x_1)\omega(x_2)/\Omega, \tag{59}$$

$$\hat{T} = 1, \tag{60}$$

$$\hat{v}_1 = \frac{1}{\hat{p}_a}\frac{d\hat{p}_a}{dx_1}u_{\rm PG}\left(x_2;\frac{\rm Kn}{\hat{p}_a(x_1)},\hat{g}\right), \tag{61}$$

$$\hat{q}_1 = \frac{d\hat{p}_a}{dx_1}Q_{\rm PG}\left(x_2;\frac{\rm Kn}{\hat{p}_a(x_1)},\hat{g}\right). \tag{62}$$

The mass flow rate M [Eq. (15)] and the heat flow rate H [Eq. (16)] are given as

$$\frac{M}{2p_0(2RT_0)^{-1/2}L} = \frac{d\hat{p}_a}{dx_1}m_{\rm PG}\left(\frac{\rm Kn}{\hat{p}_a(x_1)},\hat{g}\right), \tag{63}$$

$$\frac{H}{p_0(2RT_0)^{1/2}L} = \frac{d\hat{p}_a}{dx_1}h_{\rm PG}\left(\frac{\rm Kn}{\hat{p}_a(x_1)},\hat{g}\right), \tag{64}$$

where

$$m_{\rm PG}(K,\hat{g}) = \Omega^{-1}\int_0^1\omega(x_2)u_{\rm PG}(x_2;K,\hat{g})\,dx_2, \tag{65}$$

$$h_{\rm PG}(K,\hat{g}) = \int_0^1 Q_{\rm PG}(x_2;K,\hat{g})\,dx_2. \tag{66}$$

Here $m_{\rm PG}$ may be called the mass flow rate coefficient and $h_{\rm PG}$ the heat flow rate coefficient. The average density ρ_a of the gas at a cross section is given as

$$\frac{\rho_a}{\rho_0} = \frac{1}{\rho_0 L}\int_0^L \rho\,dX_2 = \hat{p}_a, \tag{67}$$

and thus the fraction ${\rm Kn}/\hat{p}_a$ in the arguments of $u_{\rm PG}$, $m_{\rm PG}$, etc., is expressed as

$$\frac{\rm Kn}{\hat{p}_a} = \frac{\ell_a}{L}, \tag{68}$$

where $\ell_a = 1/(\sqrt{2}\pi d_m^2 m^{-1}\rho_a)$ is the mean-free path of the gas in the equilibrium state at rest with the density ρ_a and will be called the *local* mean-free path. It should be noted that the gas is not in the equilibrium state at rest with the density ρ_a at $X_1 = X_1$. Here ℓ_a is just a measure of the gas rarefaction at each cross section through the averaged quantity ρ_a. Correspondingly, $\ell_a/L = {\rm Kn}/\hat{p}_a$ will be called the local Knudsen number.

Integrating the Boltzmann equation (2) with respect to $\boldsymbol{\zeta}$ and subsequently to x_2 from 0 to 1 and taking the boundary conditions (5) and (6) into account, we obtain the conservation of mass:

$$\frac{d}{dx_1}\left\{m_{\rm PG}\left(\frac{\rm Kn}{\hat{p}_a(x_1)},\hat{g}\right)\frac{d\hat{p}_a(x_1)}{dx_1}\right\} = 0. \tag{69}$$

This equation guarantees that the mass flow rate Eq. (63) is independent of x_1. Equation (69) is similar to the generalized Reynolds equation [35].

The solution is constructed as follows. Suppose that the boundary value problem (42) and (43) is solved for a wide range of K and $\hat{g}$ so that the database of the function $m_{\rm PG}(K,\hat{g})$ is known. Then Eq. (69) becomes an equation that determines the average pressure distribution $\hat{p}_a(x_1)$ along the channel. This is an ordinary differential equation to be solved together with Eq. (59) if the pressures $\hat{p}$ at two points on the cross sections with different x_1's are specified. Once the average pressure $\hat{p}_a(x_1)$ is known, the macroscopic variables are immediately given by Eqs. (59)–(64).

To summarize, in the Poiseuille flow problem in the presence of a finite gravity field, where the gas pressure varies not only in the flow direction but also in the vertical direction, the solution is given in a semianalytical form [Eqs. (59)–(64)] in terms of the average pressure $\hat{p}_a$. The average pressure $\hat{p}_a$ is determined by Eq. (69) once the database of $m_{\rm PG}(K,\hat{g})$ is known. Thus, the problem is reduced to solving the boundary

value problem (42) and (43) of the spatially one-dimensional linearized Boltzmann equation and obtaining the coefficient functions $u_{\rm PG}$,$m_{\rm PG}$, etc., as in the case of the conventional Poiseuille flow problem in the absence of gravity. It may be noted that the present solution [Eqs. (59)–(64)] together with Eq. (69) has the same form as that of the conventional Poiseuille flow (Refs. [30,32]) except for the additional factor $\omega(x_2)/\Omega$ in Eq. (59); the average pressure in the former plays the role of the pressure in the latter. The boundary value problem (42) and (43) is an extension of that of the conventional Poiseuille flow problem to the present problem. The characteristics are that (i) it contains the gravity term and that (ii) the variable coefficient $\omega(x_2)$ appears in the collision term. The latter means that the substantial Knudsen number varies in the vertical direction. The boundary value problem (42) and (43) is characterized by the two parameters K and $\hat{g}$ and will be solved numerically. In the next section, we show the results of the numerical analysis for various values of K and $\hat{g}$.

IV. RESULTS OF NUMERICAL ANALYSIS

A. Some comments on the numerical method

In the numerical analysis of the boundary value problem (42) and (43), we assume that the gas is a hard sphere molecular gas. The linearized collision integral (31) is then given as

$$\mathcal{L}(\phi) = \int_{\text{all } \boldsymbol{\zeta}_*} \kappa(\boldsymbol{\zeta},\boldsymbol{\zeta}_*)\phi(\boldsymbol{\zeta}_*)\, d\boldsymbol{\zeta}_* - \nu_L(\boldsymbol{\zeta})\phi(\boldsymbol{\zeta}), \tag{70}$$

where

$$\kappa(\boldsymbol{\zeta},\boldsymbol{\zeta}_*) = \frac{1}{\sqrt{2}\pi}\left[\frac{1}{|\boldsymbol{\zeta}_*-\boldsymbol{\zeta}|}\exp\left(\frac{|\boldsymbol{\zeta}_*\times\boldsymbol{\zeta}|^2}{|\boldsymbol{\zeta}_*-\boldsymbol{\zeta}|^2}\right) - \frac{|\boldsymbol{\zeta}_*-\boldsymbol{\zeta}|}{2}\right]\exp(-\boldsymbol{\zeta}_*^2), \tag{71}$$

$$\nu_L(\boldsymbol{\zeta}) = \frac{1}{2\sqrt{2}}\left[\exp(-\zeta^2) + \left(2\zeta+\frac{1}{\zeta}\right)\int_0^{\zeta}\exp(-\zeta_*^2)\mathrm{d}\zeta_*\right], \tag{72}$$

and $\zeta = |\boldsymbol{\zeta}|$.

The numerical method of a linearized Boltzmann equation has been well established in the 1980s and 1990s. Thus, we only briefly outline the numerical analysis. The boundary value problem (42) and (43) is solved using a finite difference method. The collision integral (70) is evaluated by means of the numerical kernel method [36]. A characteristic of the boundary value problem (42) and (43) is that the perturbed velocity distribution function Φ is discontinuous across the curve

$$x_2 + \frac{\zeta_2^2}{2\hat{g}} = 1 \quad (\zeta_2 < 0). \tag{73}$$

The numerical method of the Boltzmann equation having a discontinuity has been studied in Refs. [37–39], and a hybrid method of the finite difference and the characteristic coordinate methods has been developed. The numerical kernel and the hybrid methods are combined in Ref. [40]. We can apply the method to the present analysis without any major modification. The condition of the computation and the result of accuracy tests are summarized in Appendix.

B. Results of numerical analysis

In this subsection, the numerical solution for a hard sphere molecular gas are presented. As shown in Eqs. (61)–(64), the flow velocity $\hat{v}_1$, the heat flow $\hat{q}_1$, the mass flow rate M, and the heat flow rate H are expressed in terms of $u_{\rm PG}$ [Eq. (51)], $Q_{\rm PG}$ [Eq. (52)], $m_{\rm PG}$ [Eq. (65)], and $h_{\rm PG}$ [Eq. (66)], respectively. In what follows, we show the numerical results of the profiles of $u_{\rm PG}$ and $Q_{\rm PG}$ and the values of $m_{\rm PG}$ and $h_{\rm PG}$ for various sets of values of K and $\hat{g}$. In the following discussion, when we compare two $u_{\rm PG}$ for the same K and different $\hat{g}$, it may be interpreted, for example, as follows: We prepare two flows subject to gravity of different strength, control the flows to make the local density ρ_a and the normalized gradient $(L/p_a)(dp_a/dX_1)$ of the average pressure the same for the two flows at a cross section (say, $X_1 = 0$), and compare the velocity profiles of the two flows at the cross section. Similarly, when we compare two $m_{\rm PG}$, we compare the mass flows rates of the two Poiseuille flows that are subject to gravity of different strength and are made to have the same mean density and the same gradient dp_a/dX_1 of the average pressure at a cross section. Similar comments apply to $Q_{\rm PG}$ and $h_{\rm PG}$. Incidentally, for the Navier–Stokes equation under the corresponding condition of spatial variation in Sec. III, $u_{\rm PG}$ and $m_{\rm PG}$ for the leading order are given as

$$u_{\rm PG} = -\frac{1-\exp(-2\hat{g}x_2) - [1-\exp(-2\hat{g})]x_2}{2\sqrt{\pi}\gamma_1\hat{g}^2\Omega K}, \tag{74}$$

$$m_{\rm PG} = -\frac{[1-\exp(-2\hat{g})][(1+\hat{g})\exp(-2\hat{g}) - (1-\hat{g})]}{8\sqrt{\pi}\gamma_1\Omega\hat{g}^4 K}, \tag{75}$$

where the viscosity μ of the gas is connected with the mean-free path ℓ of the gas in the equilibrium state at rest with the pressure p and the temperature T as $\mu = (\sqrt{\pi}/2)\gamma_1 p(2RT)^{-1/2}\ell$, and γ_1 is a constant determined by the molecular model, e.g., $\gamma_1 = 1.270042$ for a hard sphere gas. Naturally, these expressions reduce to the well-known results

$$u_{\rm PG} = -x_2(1-x_2)/(\sqrt{\pi}\gamma_1 K) \quad \text{and} \quad m_{\rm PG} = -1/(6\sqrt{\pi}\gamma_1 K) \tag{76}$$

of the conventional Poiseuille flow as $\hat{g} \to 0$.

We first show the velocity profile of the gas. We show $u_{\rm PG}$ [Eq. (51)] for three local Knudsen numbers $K = 0.1, 1$, and 10 for various values of dimensionless gravity in Fig. 1. The case $\hat{g} = 0$ is the conventional Poiseuille flow in the absence of gravitation [10], where the velocity profile is symmetric with respect to $x_2 = 1/2$. When the Knudsen number K is relatively small [$K = 0.1$, Fig. 1(a)], the velocity profile forms a parabolic-like profile with slips on the boundaries. As the strength of gravity $\hat{g}$ increases, the velocity slip on the upper wall $x_2 = 1$ increases and that on the lower wall $x_2 = 0$ decreases as well. This trend is because the density of the gas on the upper wall decreases owing to gravity, and the substantial mean-free path increases to enhance the velocity slip there. Similarly, corresponding argument applies to the

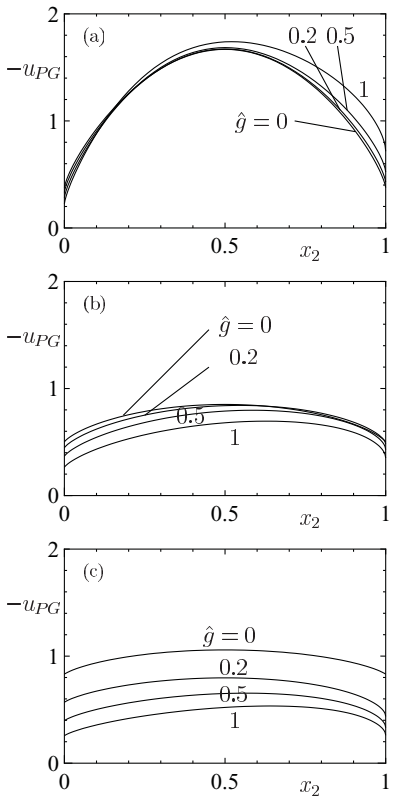

FIG. 1. Velocity profile $u_{\rm PG}$ [Eq. (51)]. (a) $K = 0.1$, (b) 1, and (c) 10. The case $\hat{g} = 0$ is the conventional Poiseuille flow in the absence of gravitation [10].

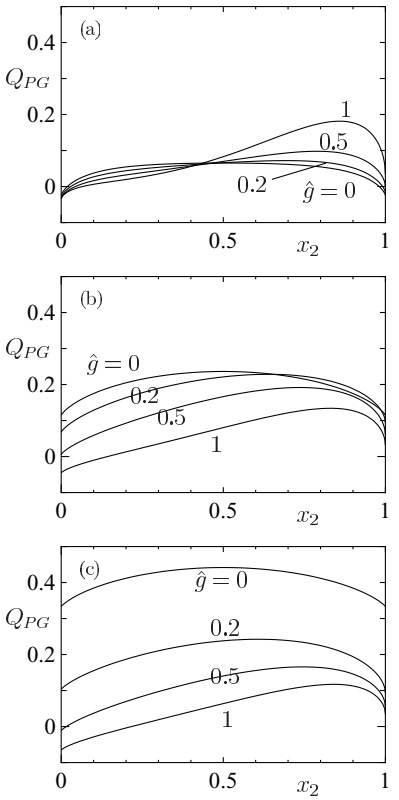

FIG. 2. Heat flow profile $Q_{\rm PG}$ [Eq. (52)]. (a) $K = 0.1$, (b) 1, and (c) 10. The case $\hat{g} = 0$ is the conventional Poiseuille flow in the absence of gravitation [10].

lower wall. The velocity profile ceases to be symmetric, and the maximum speed point x_2 shifts to a slightly upper side ($x_2 > 1/2$). The influence of gravity on the velocity profile is relatively small. As the Knudsen number increases [$K = 1$, Fig. 1(b)], the influence of gravity on the velocity profile becomes larger. The tendency of the velocity slip on the upper wall previously stated ceases to hold. Instead, the flow velocity in the bulk of the gas decreases, especially in the lower side ($x_2 < 1/2$). When the Knudsen number is large [$K = 10$, Fig. 1(c)], the decrease in the flow velocity owing to gravity is significant. This may be understood as follows. In a Poiseuille flow of a highly rarefied gas in the absence of gravitation, the perturbed velocity distribution function is composed of molecules that fly almost parallel to the walls. These molecules can arrive from a great distance, and thus the summation of the momentum amounts considerable, to results in a large macroscopic velocity. When gravity is present, on the other hand, these molecules decrease in numbers because gravity causes the molecules to fall, so that the contribution of the molecules arriving from a far distance diminishes. Consequently, the macroscopic flow velocity decreases.

Similarly, the profile $Q_{\rm PG}$ of the heat flow is shown in Fig. 2. As is well known, there is a heat flow in a rarefied gas in general even though the temperature of the gas is uniform [30]. The heat flow in the Poiseuille flow in the absence of gravity is discussed in Ref. [10]; the profile $Q_{\rm PG}$ is symmetric with respect to $x_2 = 1/2$, and the heat flow is in the same direction ($Q_{\rm PG} > 0$) as that of the pressure gradient. [For a sufficiently small Knudsen number, however, the heat flow is in the opposite direction ($Q_{\rm PG} < 0$) in the thin layers adjacent to the walls. See the case $\hat{g} = 0$ in Fig. 2(a).] For a relatively small Knudsen number [Fig. 2(a)], as the strength of gravity increases, the profile ceases to be symmetric, and a peak of $Q_{\rm PG}$ is formed at a higher position in x_2. For intermediate and large Knudsen numbers [Figs. 2(b) and 2(c)], $Q_{\rm PG}$ decreases as the strength of gravity increases, especially in the lower half part ($x_2 < 1/2$) of the channel, and for a sufficiently large $\hat{g}$, there appears a region adjacent to the lower wall ($x_2 = 0$) in which the direction of the heat flow changes ($Q_{\rm PG} < 0$).

Next, we show the mass flow rate coefficient $m_{\rm PG}$ as a function of the local Knudsen number K and the dimensionless gravity $\hat{g}$ in Table I and Fig. 3. The presence of gravitation reduces $m_{\rm PG}$ or the mass flow rate in the sense stated at the beginning of Sec. IV B. The effect of gravity on $m_{\rm PG}$ becomes significant as the local Knudsen number K increases.

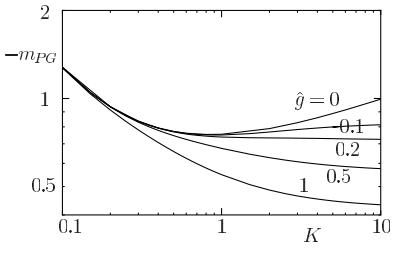

FIG. 3. Mass flow rate coefficient $m_{\rm PG}$ [Eq. (65)] as a function of K for various $\hat{g}$. The case $\hat{g} = 0$ is the conventional Poiseuille flow in the absence of gravitation [10].

TABLE I. Mass flow rate coefficient m_{PG} as a function of K and $\hat{g}$ (hard sphere gas).

	$-m_{PG}$				
K	$\hat{g}=0$[a]	0.1	0.2	0.5	1
0.1	1.278	1.278	1.278	1.277	1.272
0.2	0.9370	0.9371	0.9371	0.9363	0.9137
0.3	0.8364	0.8364	0.8361	0.8302	0.7813
0.4	0.7932	0.7931	0.7920	0.7785	0.7075
0.5	0.7719	0.7715	0.7693	0.7470	0.6591
0.6	0.7610	0.7601	0.7564	0.7252	0.6246
0.8	0.7535	0.7514	0.7439	0.6957	0.5786
1	0.7548	0.7507	0.7388	0.6760	0.5492
2	0.7892	0.7686	0.7337	0.6279	0.4864
3	0.8267	0.7836	0.7320	0.6080	0.4644
4	0.8597	0.7932	0.7305	0.5971	0.4533
5	0.8886	0.7996	0.7292	0.5902	0.4466
6	0.9142	0.8040	0.7281	0.5855	0.4421
8	0.9582	0.8097	0.7263	0.5794	0.4365
10	0.9950	0.8131	0.7251	0.5757	0.4332

[a]Reference [10].

This is well understood from the behavior of the velocity profiles in Fig. 1. In the absence of gravitation, it is well known that the mass flow rate of a Poiseuille flow exhibits the minimum at a Knudsen number around 1 (Knudsen minimum, $K \sim 0.88$ for a hard sphere molecular gas). As the strength of gravity increases, the minimum point shifts to a larger Knudsen number, i.e., $K \sim 0.90$ for $\hat{g} = 0.1$. For a larger $\hat{g}$ ($\hat{g} \geqslant 0.2$), we cannot find the minimum of m_{PG} in the range $0.1 \leqslant K \leqslant 10$.

Similarly, the heat flow rate coefficient h_{PG} is shown in Fig. 4. In the Poiseuille flow in the absence of gravity, the heat flow rate h_{PG} is a monotonically increasing function of the Knudsen number K. As the strength of gravity increases, h_{PG} decreases except for very small Knudsen numbers K (For $K = 0.1$, h_{PG} increases slightly as $\hat{g}$ increases from 0 to 1). The decrease in h_{PG} is significant for a large Knudsen number as in the case of the mass flow rate m_{PG}. For a sufficiently large $\hat{g}$, h_{PG} exhibits the maximum at an intermediate Knudsen number K.

V. FLOW THROUGH A LONG CHANNEL

In this section, we recall the original problem of this paper, i.e., the plane Poiseuille flow through a long channel, and conduct a direct numerical analysis of this flow. The aim of this section is to verify the validity of the asymptotic solution in Sec. III by comparing the result of the asymptotic solution with the numerical solution given in this section.

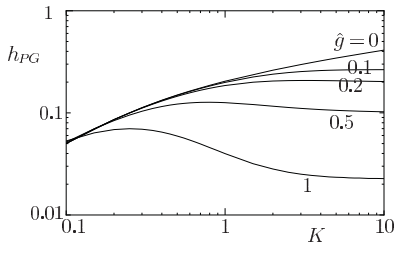

FIG. 4. Heat flow rate coefficient h_{PG} [Eq. (66)] as a function of K for various $\hat{g}$. The case $\hat{g} = 0$ is the conventional Poiseuille flow in the absence of gravitation [10].

In this section, we consider the following slightly artificial problem that simulates the long channel flow. Consider a rarefied gas in the two-dimensional rectangular domain $-W/2 < X_1 < W/2$, $0 < X_2 < L$. A uniform gravitation $(0, -g, 0)$ is present. The upper and lower boundaries are solid boundaries. The left wall $X_1 = -W/2$ and the right wall $X_1 = W/2$ are composed of the condensed phase of the gas, on which gas evaporates or condenses. Let the saturated vapor densities on the left and right walls be $\rho_A \exp(-2gX_2/L)$ and $\rho_B \exp(-2gX_2/L)$, respectively, where ρ_A and ρ_B are some constants. If we impose a difference between ρ_A and ρ_B, evaporation and condensation occur on the side boundaries, and a flow is induced. We will investigate the flow for a large aspect ratio W/L. In the numerical analysis, we employ the Boltzmann-Krook-Welander (BKW or BGK) model equation of the Boltzmann equation [41,42]. In a numerical analysis of a rarefied gas flow in general, Bird's direct simulation Monte Carlo (DSMC) method [43] is widely used, and it is of course applicable to the present problem. In this study, however, we examine the quantities of the order of $\varepsilon(\sim \hat{p}^{-1}|\partial\hat{p}/\partial x_1|) \ll 1$, and thus the numerical error should be much less than ε. Here we choose $\varepsilon \sim 0.02$, and such a delicate analysis will be difficult using the DSMC method. The BKW model is convenient for such purposes and has been applied to various studies.

The time-independent BKW (BGK) model of the Boltzmann equation for the spatially two-dimensional case is written in the dimensionless form (Sec. II) as

$$\zeta_1 \frac{\partial \hat{f}}{\partial x_1} + \zeta_2 \frac{\partial \hat{f}}{\partial x_2} - \hat{g} \frac{\partial \hat{f}}{\partial \zeta_2} = \frac{2}{\sqrt{\pi}\,\mathrm{Kn}} \hat{\rho}(\hat{f}_e - \hat{f}), \tag{77}$$

$$\hat{f}_e = \frac{\hat{\rho}}{(\pi \hat{T})^{3/2}} \exp\left[-\frac{(\zeta_i - \hat{v}_i)^2}{\hat{T}}\right], \tag{78}$$

where we choose the reference density ρ_0 as $\rho_0 = \rho_A$, and thus the mean-free path ℓ_0 of the gas is given by $\ell_0 = (8RT_0/\pi)^{1/2}/(A_c\rho_A)$, in which A_c is a constant ($A_c\rho$ is the collision frequency for the BKW model). The definition of $\hat{\rho}$, $\hat{v}_i$, $\hat{T}$ is the same as Eqs. (8)–(10). The boundary conditions on the lower and upper walls are the same as Eqs. (5) and (6). The boundary conditions on the "inlet" and "outlet" are

$$\hat{f} = \exp(-2\hat{g}x_2)E(\boldsymbol{\zeta}) \quad (x_1 = -W/2L, \zeta_1 > 0), \tag{79}$$

$$\hat{f} = (\rho_B/\rho_A)\exp(-2\hat{g}x_2)E(\boldsymbol{\zeta}) \quad (x_1 = W/2L, \zeta_1 < 0). \tag{80}$$

The boundary value problem, Eqs. (77), (5), (6), (79), and (80), is characterized by the following four dimensionless parameters

$$\mathrm{Kn} = \frac{\ell_0}{L}, \quad \hat{g} = \frac{gL}{2RT_0}, \quad \frac{\rho_B}{\rho_A}, \quad \text{and} \quad \frac{W}{L}. \tag{81}$$

Following the standard method in Ref. [44], we can eliminate the molecular velocity component ζ_3 from the boundary value problem. This reduced problem, which is a problem with four independent variables $x_1, x_2, \zeta_1, \zeta_2$, is solved using a finite difference method. Like the boundary value problem (42)

and (43), the velocity distribution function is discontinuous across the following surface in the three-dimensional space of x_1, x_2, ζ_2:

$$x_1 + \frac{\zeta_1\zeta_2}{\hat{g}} = s, \quad x_2 + \frac{\zeta_2^2}{2\hat{g}} = 1 \quad (\zeta_2 < 0), \tag{82}$$

where $-W/2L \leqslant s \leqslant W/2L$ and $-\infty < \zeta_1 < \infty$. The numerical method of a two-dimensional model Boltzmann equation with an external force has been developed in Ref. [45]. We can apply the method with a small modification at the side boundaries (79) and (80).

The two-dimensional problem considered in this section contains artificial boundaries, and thus there are inevitable end effects near the side boundaries $x_1 = -W/2L$ and $x_1 = W/2L$. We confirm from the numerical solution that the end effects vanish if we are sufficiently apart from the side boundaries. Whether the end effect vanishes is judged in the following way. According to the asymptotic solution, the ratio $(\partial\hat{p}/\partial x_1)/\hat{p}$ is independent of x_2 up to the order of ε [Eq. (59)]. From the numerical data, we judge that the end effect vanishes at the cross section x_1 if the variation of $(\partial\hat{p}/\partial x_1)/\hat{p}$ with respect to x_2 is of the order of ε^2. To be specific, we compute the ratio $\Delta(x_1) = |\max_{x_2}\psi - \min_{x_2}\psi|/\psi^2$ with $\psi = (\partial\hat{p}/\partial x_1)/\hat{p}$, where the denominator is a measure of ε^2, and judge that the previously stated condition is satisfied if $\Delta \leqslant 0.1$. We show an example of this test in Fig. 5. In Fig. 5, the variation of Δ is shown as a function of x_1 for three computational conditions $(W/L, \rho_B/\rho_A) = (10,0.8),(20,0.6)$, and (40, 0.2) and $\mathrm{Kn} = 1$ and $\hat{g} = 1$. As we see in Fig. 5, the end effects vanish, and the numerical solution satisfy the property of the asymptotic solution in a wide central region if W/L is large. From this test, we choose $W/L = 40$ and $\rho_B/\rho_A = 0.2$ in the following analysis.

We carry out the verification of the asymptotic solution in the following way:

(i) Set the parameters Eq. (81) and obtain the solution.

(ii) Fix K and find the position x_1 at which $\mathrm{Kn}/\hat{p}_a(x_1)$ (local Knudsen number) $= K$.

(iii) Obtain the density $\hat{\rho}$, flow velocity $\hat{v}_1$, and the pressure $\hat{p}$ at this x_1 using an interpolation and compute the ratios $(\hat{p}_a^{-1}d\hat{p}_a/dx_1)^{-1}\hat{v}_1$ and $(d\hat{p}_a/dx_1)^{-1}M/[2p_0(2RT_0)^{-1/2}L]$. Compare them with $u_{\mathrm{PG}}(x_2; K, \hat{g})$ and $m_{\mathrm{PG}}(K, \hat{g})$ [cf. Eqs. (61) and (63)].

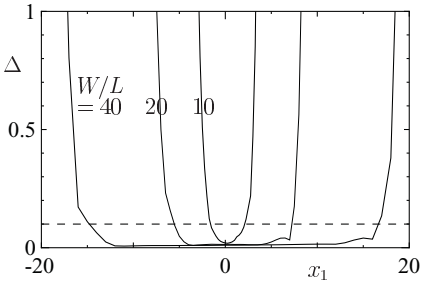

FIG. 5. Test of the end effects ($\mathrm{Kn} = 1$ and $\hat{g} = 1$). $\Delta = |\max_{x_2}\psi - \min_{x_2}\psi|/\psi^2$ with $\psi = (\partial\hat{p}/\partial x_1)/\hat{p}$ as a function of x_1 for three computational conditions $(W/L, \rho_B/\rho_A) = (10,0.8),(20,0.6)$, and $(40, 0.2)$. Dotted line: $\Delta = 0.1$. The end effects are judged to vanish when the solid line is below the dotted line.

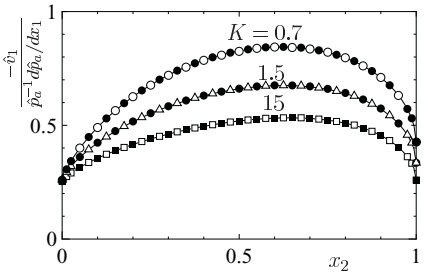

FIG. 6. Verification test of the asymptotic solution I: velocity profile ($\hat{g} = 1$). Markers show the normalized flow velocity $(\hat{p}_a^{-1}d\hat{p}_a/dx_1)^{-1}\hat{v}_1$ at the local Knudsen number $\mathrm{Kn}/\hat{p}_a = K$ taken from the two-dimensional solutions for the following cases: open circle (◯): $\mathrm{Kn} = 0.1$; closed circle (●): $\mathrm{Kn} = 0.2$; open triangle (△): $\mathrm{Kn} = 0.5$; open square(□): $\mathrm{Kn} = 2$; and closed square (■): $\mathrm{Kn} = 5$. Solid line (——): asymptotic solution $-u_{\mathrm{PG}}$ for the BKW model [see Eq. (61)].

(iv) Repeat (ii) and (iii) for other values of K in the range where Δ satisfies the condition stated in the previous paragraph.

(v) Repeat the processes (i)–(iv) for other set of the parameters (81).

Some examples of this test are shown as follows. The computation is carried out for the 24 combinations of $\mathrm{Kn} = 0.1,0.2,0.5,1,2$, and 5 and $\hat{g} = 0.1,0.2,0.5$, and 1. We show the normalized flow velocity profiles $(\hat{p}_a^{-1}d\hat{p}_a/dx_1)^{-1}\hat{v}_1$ in Fig. 6 for $\hat{g} = 1$ and three values of K. Markers show the profile of the two-dimensional solutions that are taken from five solutions with $\hat{g} = 1$ and $\mathrm{Kn} = 0.1,0.2,0.5,2$, and 5, and different markers represent solutions with different Kn. The solid line represent the $-u_{\mathrm{PG}}$ for the BKW model. We see that the normalized velocity profiles $(\hat{p}_a^{-1}d\hat{p}_a/dx_1)^{-1}\hat{v}_1$ of the two-dimensional solution are determined by K and $\hat{g}$ irrespective of the parameters (81) and coincide with u_{PG} of the asymptotic solution [cf. Eq. (61)]. In Fig. 7 we show the relation between the normalized mass flow rate $(d\hat{p}_a/dx_1)^{-1}M/[2p_0(2RT_0)^{-1/2}L]$ and the local Knudsen number K at various x_1. Again, markers show the two-dimensional solution and different markers correspond to the

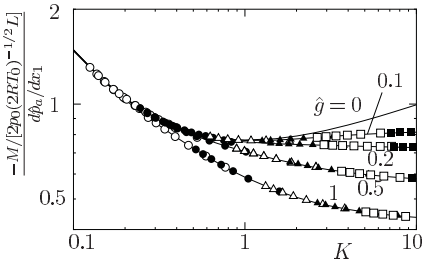

FIG. 7. Verification test of the asymptotic solution II: mass flow rate. Markers show the normalized mass flow rate $(d\hat{p}_a/dx_1)^{-1}M/[2p_0(2RT_0)^{-1/2}L]$ at the local Knudsen number $\mathrm{Kn}/\hat{p}_a = K$ taken from the two-dimensional solutions for the following cases: open circle (◯): $\mathrm{Kn} = 0.1$; closed circle (●): $\mathrm{Kn} = 0.2$; open triangle (△): $\mathrm{Kn} = 0.5$; closed triangle (▲): $\mathrm{Kn} = 1$; open square(□): $\mathrm{Kn} = 2$; and closed square(■): $\mathrm{Kn} = 5$. Solid line: asymptotic solution $-m_{\mathrm{PG}}$ for the BKW model [see Eq. (63)]. The meaning of the markers is the same as that in Fig. 6.

solutions with different Kn. The solid line is the $-m_{\rm PG}$ for the BKW model. From Fig. 7, we see that the the normalized mass flow rate $(d\hat{p}_a/dx_1)^{-1}M/[2p_0(2RT_0)^{-1/2}L]$ of the two-dimensional solution is determined by K and $\hat{g}$ irrespective of the parameters (81) and coincide with $m_{\rm PG}(K,\hat{g})$ of the asymptotic solution [cf. Eq. (63)]. From the test, we may conclude that the solution in the central part of the channel of the two-dimensional problem for a large aspect ratio W/L is well expressed by the asymptotic solution.

VI. CONCLUSION

In this study, we considered a plane Poiseuille flow of a rarefied gas that flows horizontally in the presence of strong gravitation based on the Boltzmann equation. Applying the asymptotic analysis of the Boltzmann equation for a small variation in the flow direction, the two-dimensional problem is reduced to a one-dimensional problem, as in the case of a Poiseuille flow in the absence of gravitation, and the solution is obtained in a semianalytical form. The reduced one-dimensional problem is solved numerically for a hard sphere molecular gas over a wide range of the local Knudsen number and dimensionless gravity. The presence of gravitation reduces the mass flow rate (see Sec. IV B), and the effect of gravitation is significant for large Knudsen numbers. To verify the asymptotic solution, we also conducted a direct numerical analysis of a two-dimensional flow through a long channel. By comparing the asymptotic solution with the direct numerical solution, the validity of the asymptotic solution is confirmed.

In this study, we considered uniform gravitation g that is independent of the vertical coordinate X_2. To loosen this condition such that the external force is an arbitrary function of X_2 is straightforward. The basic result in Sec. III is unchanged except that the density function $\omega(x_2)$ [Eq. (29)] as well as its integral Ω [Eq. (34)] and the solution of the one-dimensional problem (42) and (43) change.

APPENDIX: COMPUTATIONAL CONDITION AND ACCURACY TESTS

The computational condition and the results of accuracy tests are summarized here.

For the one-dimensional problem in Sec. IV, the computational condition is as follows. The computation is carried out in the finite three-dimensional space $0 \leqslant x_2 \leqslant 1$, $-\zeta_D \leqslant \zeta_2 \leqslant \zeta_D$, and $0 \leqslant \zeta_\rho \leqslant \zeta_D$, where $\zeta_D = 3.9$. In the interval $0 \leqslant x_2 \leqslant 1$, 241 lattice points with a nonuniform lattice size are put. The lattice size is minimum (0.0021) around $x_2 = 0$ and $x_2 = 1$, maximum (0.005) and uniform in the interval $0.16 \leqslant x_2 \leqslant 0.84$, and nonuniform otherwise. For the molecular velocity, 385 lattice points with the uniform size are put in $-\zeta_D \leqslant \zeta_2 \leqslant \zeta_D$ and 33 lattice points with the uniform size in $0 \leqslant \zeta_\rho \leqslant \zeta_D$.

The results of the accuracy tests are as follows:

(i) Choice of ζ_D. The magnitude of the substantial distribution function $|\Phi|E$ on the planes $\zeta_2 = \pm\zeta_D$ and $\zeta_\rho = \zeta_D$ is less than 3.4×10^{-6}.

(ii) Conservation law. Multiplying the Boltzmann equation Eq. (42) by $\zeta_1^2 E$, integrating with respect to $\boldsymbol{\zeta}$ for its entire space, and integrating with respect to x_2 from 0 to x_2, we have the conservation of momentum:

$$\frac{1}{\sqrt{\pi}}\left[\omega(x_2)\int_{-\infty}^{\infty}\int_{0}^{\infty}\zeta_2\zeta_\rho^3\Phi\exp(-\zeta_2^2-\zeta_\rho^2)\,d\zeta_\rho\,d\zeta_2\right]_0^{x_2} + \frac{1}{4\hat{g}}[1-\exp(-2\hat{g}x_2)] = 0.$$

The left-hand side, which should vanish theoretically, is confirmed to be less than 5.3×10^{-4} except for the cases $(K,\hat{g}) = (0.1,0.1)$ and $(0.2,0.1)$, for which less than 1.5×10^{-3}.

(iii) Recomputation on another lattice system. For a test of accuracy, recomputation using a coarser lattice system is carried out, i.e., about 1.5 times coarser in x_2, ζ_2, and ζ_ρ, for all the cases of Kn and $\hat{g}$ shown in Table 1. From the test, the numerical error in Table 1 is estimated to be less than 0.024%.

For the two-dimensional problem in Sec. V, the computational condition is as follows. The computation is carried out in the finite four-dimensional space $-W/2L \leqslant x_1 \leqslant W/2L$, $0 \leqslant x_2 \leqslant 1$, $-\zeta_D \leqslant \zeta_1 \leqslant \zeta_D$, and $-\zeta_D \leqslant \zeta_2 \leqslant \zeta_D$. The lattice points are put uniformly for each axis. Forty-one lattice points are put in $-W/2L \leqslant x_1 \leqslant W/2L$, 81 points in $0 \leqslant x_2 \leqslant 1$, 61 points in $-\zeta_D \leqslant \zeta_1 \leqslant \zeta_D$, and 641 points in $-\zeta_D \leqslant \zeta_2 \leqslant \zeta_D$.

The results of the accuracy tests are as follows:

(i) Choice of ζ_D. The distribution function $\hat{f}$ on the planes $\zeta_1 = \pm\zeta_D$ and $\zeta_2 = \pm\zeta_D$ is less than 1.6×10^{-6}.

(ii) Recomputation on another lattice system. For a test of accuracy, recomputation using a coarser lattice system is carried out, where (a) lattices in x_2 and ζ_2 are both two times coarser and (b) lattice in x_1 is two times coarser, for the typical three cases of Kn = 0.1,1, and 10 and $\hat{g} = 1$. The normalized mass flow rate $(d\hat{p}_a/dx_1)^{-1}M/[2p_0(2RT_0)^{-1/2}L]$ computed from the standard and the additional computations (a) and (b) are compared for various K [see the process (iii) in Sec. V]. From this test, the numerical error in the relation between the normalized mass flow rate and the local Knudsen number is estimated to be less than 0.08%.

[1] C. Cercignani and A. Daneri, J. Appl. Phys. **34**, 3509 (1963).
[2] C. Cercignani and F. Sernagiotto, Phys. Fluids **9**, 40 (1966).
[3] J. H. Ferziger, Phys. Fluids **10**, 1448 (1967).
[4] Y. Sone and K. Yamamoto, Phys. Fluids **11**, 1672 (1968); **13**, 1651(E) (1970).
[5] S. K. Loyalka, Phys. Fluids **17**, 1053 (1974).
[6] T. Kanki and S. Iuchi, Phys. Fluids **16**, 594 (1973).
[7] S. K. Loyalka, T. S. Strovick, and H. S. Park, J. Vac. Sci. Technol. **13**, 1188 (1976).
[8] Y. Sone and M. Hasegawa, J. Vac. Soc. Jpn. **30**, 425 (1987) (in Japanese).
[9] M. Hasegawa and Y. Sone, J. Vac. Soc. Jpn. **31**, 416 (1988) (in Japanese).
[10] T. Ohwada, Y. Sone, and K. Aoki, Phys. Fluids A **1**, 2042 (1989).

[11] Y. Sone and E. Itakura, J. Vac. Soc. Jpn. **33**, 92 (1990) (in Japanese); the database is available from [http://fd.kuaero.kyoto-u.ac.jp/members/sone/].
[12] F. Sharipov and V. Seleznev, J. Phys. Chem. Ref. Data **27**, 657 (1998).
[13] F. Sharipov, J. Vac. Sci. Technol. A **17**, 3062 (1999).
[14] F. Sharipov and G. Bertoldo, Phys. Fluids **21**, 067101 (2009).
[15] S. Takata and H. Funagane, J. Fluid Mech. (2011) (to be published).
[16] M. Alaoui and A. Santos, Phys. Fluids A **4**, 1273 (1986).
[17] M. Tij and A. Santos, J. Stat. Phys. **76**, 1399 (1994).
[18] M. Malek Mansour, F. Baras, and A. L. Garcia, Physica A **240**, 255 (1997).
[19] M. Tij, M. Sabbane, and A. Santos, Phys. Fluids **10**, 1021 (1998).
[20] D. Risso and P. Cordero, Phys. Rev. E **58**, 546 (1998).
[21] S. Hess and M. Malek Mansour, Physica A **272**, 481 (1999).
[22] F. J. Uribe and A. L. Garcia, Phys. Rev. E **60**, 4063 (1999).
[23] M. Tij and A. Santos, Physica A **289**, 336 (2001).
[24] K. Aoki, S. Takata, and T. Nakanishi, Phys. Rev. E **65**, 026315 (2002).
[25] M. Sabbane, M. Tij, and A. Santos, Physica A **327**, 264 (2003).
[26] M. Tij, V. Garzó, and A. Santos, Phys. Rev. E **56**, 6729 (1997).
[27] M. Tij, V. Garzó, and A. Santos, *Rarefied Gas Dynamics*, edited by R. Brun, R. Campargue, R. Gatignol, and J.-C. Lengrand (Cépaduès, Toulouse, 1999), p. 239.
[28] M. Tij, V. Garzó, and A. Santos, Phys. Fluids **11**, 893 (1999).
[29] E. E. Tahiri, M. Tij, and V. Garzó, Physica A **297**, 97 (2001).
[30] Y. Sone, *Molecular Gas Dynamics* (Birkhäuser, New York, 2007).
[31] K. Aoki and P. Degond, Multiscale Model. Simul. **1**, 304 (2003).
[32] K. Aoki, P. Degond, S. Takata, and H. Yoshida, Phys. Fluids **19**, 117103 (2007).
[33] S. Takata, H. Sugimoto, and S. Kosuge, Euro. J. Mech. B/Fluids **26**, 155 (2007).
[34] Y. Sone and K. Aoki, J. Mec. Theor. Appl. **2**, 3 (1983).
[35] S. Fukui and R. Kaneko, J. Tribol. **110**, 253 (1988).
[36] Y. Sone, T. Ohwada, and K. Aoki, Phys. Fluids A **1**, 363 (1989).
[37] Y. Sone and H. Sugimoto, *Adiabatic Waves in Liquid-Vapor Systems*, edited by G. E. A. Meier and P. A. Thompson (Springer-Verlag, Berlin, 1990), p. 293.
[38] K. Aoki, Y. Sone, K. Nishino, and H. Sugimoto, *Rarefied Gas Dynamics*, edited by A. E. Beylich (VCH, Weinheim, 1991), p. 222.
[39] H. Sugimoto and Y. Sone, Phys. Fluids A **4**, 419 (1992).
[40] S. Takata, Y. Sone, and K. Aoki, Phys. Fluids A **5**, 716 (1993).
[41] P. L. Bhatnagar, E. P. Gross, and M. Krook, Phys. Rev. **94**, 511 (1954).
[42] P. Welander, Ark. Fys. **7**, 507 (1954).
[43] G. A. Bird, *Molecular Gas Dynamics and the Direct Simulation of Gas Flows* (Oxford University Press, Oxford, 1994).
[44] C. K. Chu, Phys. Fluids **8**, 12 (1965).
[45] Y. Sone, K. Aoki, and H. Sugimoto, Phys. Fluids **9**, 3898 (1997).